THE JOURNAL OF PHYSICAL CHEMISTRY B

Article

pubs.acs.org/JPCB

Hydrogen Atom in Water from Ambient to High Temperatures

Anna Pomogaeva[§] and Daniel M. Chipman*

Radiation Laboratory, University of Notre Dame, Notre Dame, Indiana 46556-5674, United States

Supporting Information

ABSTRACT: The aqueous hydrogen atom is studied with molecular dynamics simulations from ambient temperature to near the critical point. The radial distribution functions find a hydrogen atom coordination number of about 13 water molecules at 300 K to about 4 water molecules at 646 K. The radial and angular distribution functions indicate that first-shell water molecules tend to orient to maximize hydrogen bonding interactions with other water molecules. These orientational tendencies diminish with temperature. The calculated diffusion coefficient agrees very well with experimental results known near ambient temperatures. It fits a simple activation model to about 575 K, above which the diffusion becomes much faster than predicted by the fit. To temperatures of at least 500 K there is evidence for caging on a time scale of about 1 ps, but the evidence disappears at very high temperatures. Values of the aqueous hydrogen hyperfine coupling constant are obtained by averaging the results of density functional calculations on clusters extracted from the simulations. The hyperfine coupling calculations do not agree well with experiment for reasons that are not understood now, pointing to the need for further research on this problem.

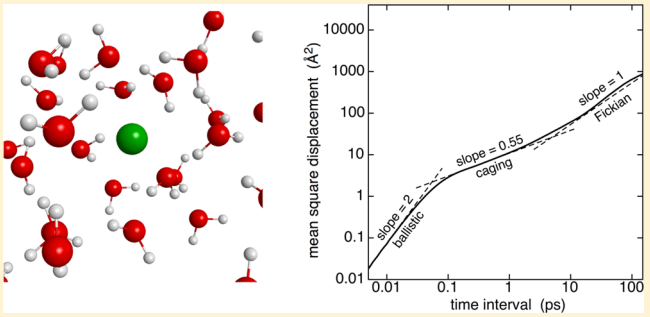

INTRODUCTION

The hydrogen atom is a primary product in the radiolysis of water,[1,2] where its production increases substantially with photon energy[3] and with temperature.[4] A number of its important aqueous reactions have been studied experimentally.[5] Surprisingly for a hydrophobe, it has a diffusion constant[6] D_H of 0.77 ± 0.10 Å²/ps that is much higher than the value[7] 0.23 Å²/ps for the self-diffusion of water, approaching the value[8] of 0.93 Å²/ps for the proton in water, even though no analogous Grotthuss-like mechanism is available. Also interesting is that the electron paramagnetic resonance hyperfine coupling constant A of a hydrogen atom in water is 0.6% lower than it is in the gas phase.[9,10]

Several computational studies have been made on the structure and diffusion of a hydrogen atom in water. An early classical molecular dynamics (MD) study[11] found the hydrogen atom to be in a clathrate cage, with an effective size somewhat larger than a water molecule. Generalization to a path integral MD treatment[12] found very little effect on the structure from the quantum nature of the hydrogen nuclear motions. A later path integral Monte Carlo study[13] further found only small quantum effects on the free energy of solvation of the hydrogen atom, while, however, noting a sensitive dependence of the radial distribution function (RDF) on the solute−solvent potential adopted. A Car−Parrinello classical MD study[14] found that the solvation cavity has an effective size smaller than in previous studies, only slightly larger than a water molecule, and is highly dynamic, such that that the diffusion is mainly due to the hydrogen atom following the fast motion of its cavity, which in turn is driven by rapid structural fluctuations in the water hydrogen bonding network. A subsequent Car−Parrinello classical MD study found essentially the same features.[15] A recent study using ring polymer MD[16] also showed the effective cavity size to be only slightly larger than a water molecule and confirmed the hydrogen atom diffusion to be mainly due to its cavity diffusion, while further finding a smaller additional contribution from a hopping mechanism to be significant in a classical treatment, which is somewhat suppressed in a quantum treatment of the hydrogen nuclear motion.

Several experimental and phenomenological modeling efforts have been made to understand the behavior of the hyperfine coupling constant A in water. The first study of the temperature dependence of A in water found that the ratio A/A_{vac} in water to that in gas decreases in a linear manner from a factor of 0.9940 at 293 K to 0.9932 at 363 K.[17] This behavior was rationalized with a clathrate model wherein vibrational motions of the hydrogen atom leading to collisions with the clathrate wall allow delocalization of its spin onto neighboring water molecules, with a smaller contribution from compression of the wave function due to its confinement in the cage. A very recent work extends the study to still higher temperatures, finding that A/A_{vac} reaches a minimum of 0.9918 at 513 K and then rises with further increase in temperature to 0.9923 at 573 K.[18] The latter data was found to fit a quadratic behavior with temperature, which was rationalized by adding to the wall

Received: October 29, 2013
Revised: November 22, 2013
Published: December 3, 2013

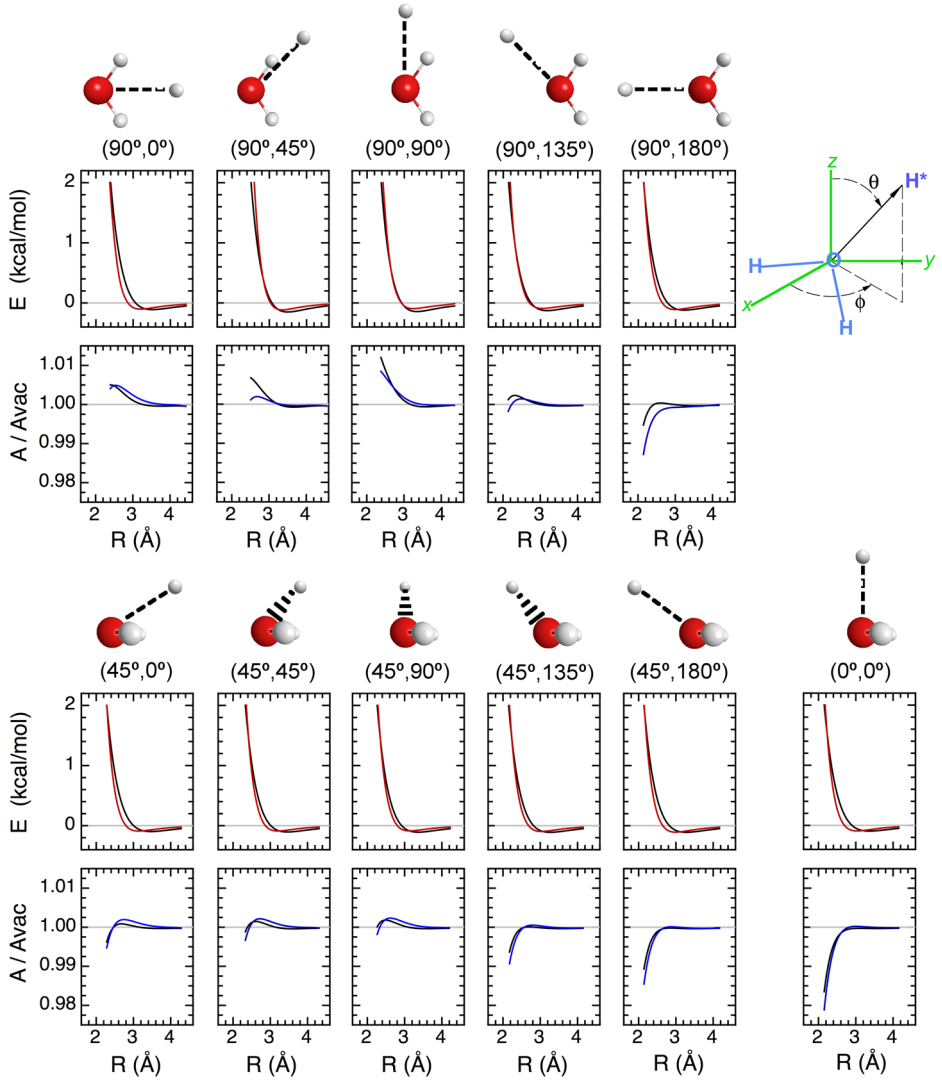

Figure 1. The panel in the upper right corner shows the spherical polar coordinate system defining geometries for the H*−W interaction. Otherwise, the panels in the first and fourth rows show geometries for the 11 rays of H* approach to W. The second and fifth rows show the corresponding CCSD(T)/aug-cc-pVTZ (black) and fitted AMOEBA (red) interaction energies in kcal/mol vs the H*−O distance in Å. The third and sixth rows show the corresponding CCSD/supp-aug-cc-pVTZ (black) and PBE40/aug-cc-pVTZ/6-31+G* (blue) hyperfine coupling ratios A/A_{vac} vs the H*−O distance in Å.

collision and compression mechanisms another effect from the wall collision frequency, where changes with temperature of the water density and the hydrogen atom partial molar volume alter the mean free path, along with a simple ansatz for the effectiveness of each collision.

In this work we use computation to examine these interesting behaviors of the hydrogen atom in water. A force field for hydrogen atom interacting with water is obtained by fitting to high level electronic structure calculations. Classical MD simulations are then carried out from ambient to high temperature to determine RDFs, angular distribution functions (ADFs), coordination numbers, and transport properties. Finally, clusters are extracted from snapshots of the MD trajectories and subjected to electronic structure calculations to determine hyperfine coupling constants. The MD simulations are carried out with the TINKER program,[19] and all electronic structure calculations use the QChem program.[20]

SIMULATION DETAILS

Force Field. The force field adopted in this work is based on the flexible polarizable AMOEBA model previously developed for water.[21−23] This model gives a good description of the neat water heat of vaporization, dielectric constant, self-diffuson constant, and radial distribution functions from ambient to supercritical conditions, provided the densities are fixed at the experimental values, provides good densities near ambient conditions, and somewhat underestimates the densities at high temperatures.[24] The basic AMOEBA recipe has also been parametrized for many solutes and shown to be very successful in describing the behavior of a large variety of neutral organic,[25−27] ionic inorganic,[25,28−34] and biochemical[25] species in water at ambient conditions.

Briefly, the AMOEBA force field describes the water flexible monomer with an equilibrium geometry having OH distance of 0.9572 Å the same as the experimental gas phase monomer and HOH angle of 108.5° that is slightly higher than the experimental gas phase monomer value of 104.5°, with

dx.doi.org/10.1021/jp4106844 | J. Phys. Chem. B 2013, 117, 16530−16541

harmonic and anharmonic force constants including Urey–Bradley terms. Permanent charges, dipoles, and quadrupoles are placed on each atom, while induced dipoles are allowed to further develop via polarizabilities assigned to each atom. The electrostatic and induction interactions use smeared multipoles to provide Thole-type[35] damping that prevents short-range polarization catastrophes. The van der Waals terms for intermolecular dispersion and exchange repulsion are described with a buffered 14–7 potential[36] on oxygen and at points on the OH bonds near the hydrogens. Properties of dimer through hexamer gas-phase water clusters as well as of bulk ambient water were considered while optimizing the various parameters.

For the case of a hydrogen atom, which has no permanent moments, the AMOEBA recipe only requires parameters for the polarizability and van der Waals interactions. The polarizability was set to the known value[37] of 4.5 a_0^3 = 0.667 Å^3. The van der Waals parameters of buffered 14–7 form[36] were determined by fitting to high-level electronic structure benchmark calculations.

To fit the van der Waals parameters, calculations were made on a hydrogen atom (H*) interacting with a single water molecule (W). The W was held at its equilibrium AMOEBA geometry, and the H* was allowed to approach it at various radial distances along rays emanating from the oxygen atom at spherical polar angles (θ,ϕ), as defined in the upper right corner panel of Figure 1. Thus, the water hydrogens (H) have spherical polar angles of (90°, ± 54.25°). Eleven symmetry-unique values of (θ,ϕ) were used, which become equivalent to 26 rays with symmetry redundancy.

Benchmark calculations of the H*–W interaction energy used the high level ab initio CCSD(T) method[38,39] with the large aug-cc-pVTZ basis set.[40,41] Corrections were made for basis set superposition error (BSSE) using the counterpoise method.[42] Along each ray, calculations were made at H*–O radial distances ranging from 2.0 to 5.0 Å. Interestingly, the H*–W interaction energy was found to have a small attractive minimum along every ray considered. The most attractive minimum among the rays considered occurs where H* approaches near a water H in the water plane at (90°, 45°) and H*–O distance of 3.49 Å, with a well depth of −0.15 kcal/mol. This is very close to the fully minimized H* position that occurs at (90°, 62°) and H*–O distance of 3.45 Å, with a well depth of −0.16 kcal/mol. The least attractive minimum among all the rays considered occurs where H* approaches the water O perpendicular to the plane at (0°, 0°) and H*–O distance of 3.36 Å, with a well depth of −0.10 kcal/mol.

Note that other metastable local minima for H* interacting with a water molecule have been reported;[43] these lie at such high energies (~16 kcal/mol) as to not play a significant role in the present study. That work also reported a number of local minimum structures for H* interacting with two to four water molecules. In all of the latter cases the only low-lying structures have essentially the same motif where H* interacts directly with only one of the water molecules just as in its global minimum interaction with water monomer. The various structures differ from one another only in the way that the water molecule directly involved with H* makes hydrogen bonds to other water molecules that are remote from H*.

The H*–W interaction energy was then evaluated with the assumed form of the AMOEBA force field at a subset of the points used for the CCSD(T)/aug-cc-pVTZ results, omitting points at short distances where the repulsive interaction energy was stronger than 2.0 kcal/mol, which varied from about 2.2 to 2.5 Å, and also omitting points at large distances where the attractive interaction energy was weaker than −0.05 kcal/mol, which varied from about 4.1 to 4.5 Å. The van der Waals parameters were varied to minimize the overall root mean square (rms) deviation of the AMOEBA results from the aforementioned subset of benchmark CCSD(T)/aug-cc-pVTZ calculations. This fitting produced van der Waals parameters of R^0 = 3.035 Å and ε = 0.0206 kcal/mol in the notation of the original AMOEBA papers.[21,22]

The second and fifth rows of Figure 1 show the benchmark CCSD(T)/aug-cc-pVTZ (black) and fitted AMOEBA (red) potential energy curves obtained along each of the 11 symmetry unique rays. The third and sixth rows show associated hyperfine coupling constant information that is discussed in a later section. While the energy fits are satisfactory in all cases, the limited functional form of the AMOEBA recipe does not allow for fully quantitative agreement. The energy fits are best at (90°, 45°), (90°, 90°), and (90°, 135°), where H* approaches in the W plane laterally. For other approaches the AMOEBA potential curves consistently show a slightly too-weak repulsion near where the inner wall begins to rise. Although regions with energies above 2 kcal/mol were not used in the fitting process, the fits remain quite good, up to well above 3 kcal/mol, albeit with slightly too-strong repulsion, beyond which trajectories are very unlikely to probe.

The force field described above was developed by fitting the two-body interactions between H* and one water molecule. Since it will subsequently be used for simulation of H* with many waters, it is of interest to check on how well it describes three-body interactions. The fairly good performance of AMOEBA for three-body interactions in neat water has been previously documented.[44] To analyze the three-body interactions when one of the bodies is H* we inspected 100 random snapshots from the 300 K simulation described below and extracted from each snapshot the coordinates of H* along with the closest two water molecules for analysis. For this collection of structures the benchmark three-body interactions from CCSD(T)/aug-cc-pVTZ with counterpoise correction for basis set superposition error ranged from −0.29 to +0.40 kcal/mol. The analogous three-body interactions from AMOEBA agreed to those from the benchmarks with a mean unsigned error of just 0.07 kcal/mol. In view of the fact that this analysis used the most challenging cases of the closest water molecules, the small three-body interactions seem to be quite satisfactorily described in general by the AMOEBA force field.

It is concluded that the AMOEBA force field should be suitable for evaluation of aqueous H* interaction energies. Still, it is useful to investigate where the most significant errors may lie. Evidently, from Figure 1, with the exception of lateral approach in the molecular plane where the fits are quite good, the errors in the AMOEBA force field are most significant for the repulsive wall. For H* having less than thermal kinetic energy the benchmarks show it should begin to feel the repulsive wall at around 2.5–2.8 Å from O, depending on the angle of approach, whereas the AMOEBA potential will allow it to come about 0.1–0.2 Å too close. Conversely, for H* having somewhat higher than thermal kinetic energy the benchmarks show it should begin to feel the repulsive wall at around 2.0–2.4 Å from O, again depending on the angle of approach, whereas the AMOEBA potential will keep it about 0.1–0.2 Å too far away. Such small discrepancies may have a noticeable influence on the calculated hyperfine coupling constants, which will be taken up in detail in a later section.

Simulation Conditions. The fitted force field was used in classical MD simulations, carried out with the same Tinker program[19] that was used to develop the AMOEBA model, adopting without change the original parameters of the model for W−W interactions. Simulations were carried out at constant particle number and constant volume. In most cases temperature was held nearly constant through velocity scaling regulated by the Berendsen weak-coupling thermostat.[45] This strictly gives an ensemble intermediate between canonical and microcanonical,[46] which with the default coupling time constant of 0.1 ps used in the calculations reported herein approaches closely to the weak coupling limit of the canonical ensemble.

Cubic boxes containing one hydrogen atom together with either 215 or 511 water molecules were considered. Since the "size" of a hydrogen atom in water is believed to be about the same as that of a water molecule, the box sizes were set to reproduce the experimental densities along the coexistence curve of bulk water for boxes that would contain either 216 or 512 water molecules, respectively. Periodic boundary conditions were invoked, using particle-mesh Ewald summation of order 8 for electrostatic interactions with a cutoff radius of 9 Å. The van der Waals interactions beyond 12 Å were tapered to zero with a 1.2 Å switching function. The equations of motion were integrated with a modified Beeman algorithm[47,48] using time steps of 1.0 fs. Induced dipoles were converged to 10^{-4} D rms. At each state point the equilibration phase was run for at least 200 ps starting from a nearby state point.

Temperatures were considered over the range from 300 K, representing ambient conditions, to 646 K, which is close to the experimental critical point of water that occurs at 647.1 K. This is well above the critical point of the AMOEBA model itself, which occurs at about 600 K.[24] The corresponding densities span a range from 0.997 to 0.403 g/cm^3.

Production trajectories were carried out in the weak coupling ensemble with 215 waters for 10 runs of 1 ns each. Some checks on the results were also made with trajectories in the weak coupling ensemble with 511 waters for 1.5 ns. Radial distribution functions, angular distribution functions, and diffusion coefficients from the 511 water runs were found to essentially agree with those from the 215 water runs to within the estimated statistical errors.

STRUCTURE

Radial Distribution Functions. Results at ambient conditions are compared to others from the literature, in Figure 2. The Markland et al.[16] study carried out both classical and ring polymer MD calculations using a nonpolarizable potential consisting of a TIP4P water variant and H*−W described with a Buckingham repulsion and damped C/R^6 attraction having parameters previously obtained[49] to fit experimental spin relaxation rates for isotopic studies of hydrogen atom diffusion in ice. The study by Kirchner et al.[14] carried out Car−Parrinello classical MD on D in D_2O using the BLYP density functional method for on-the-fly energy evaluations.

For both H*−O and H*−H, the AMOEBA RDF obtained at 300 K is in very good overall agreement with that obtained in the classical MD simulation at 315 K of Markland et al. The only notable difference is that the latter has a slightly higher first peak in each case. However, the RDFs from both AMOEBA and Markland et al. differ significantly from those obtained in the Car−Parrinello calculation at 315 K of Kirchner et al. Compared to AMOEBA and Markland et al., the Kirchner et al. RDFs have substantial amplitude at much shorter distances, for both H*−O and H*−H. For H*−O the first peak is at about the same position and height, while the first minimum and second peak occur at significantly shorter distances. For H*−H the first peak has a monomodal structure occurring at a position between the bimodal features of the other RDFs, and the first minimum has higher amplitude.

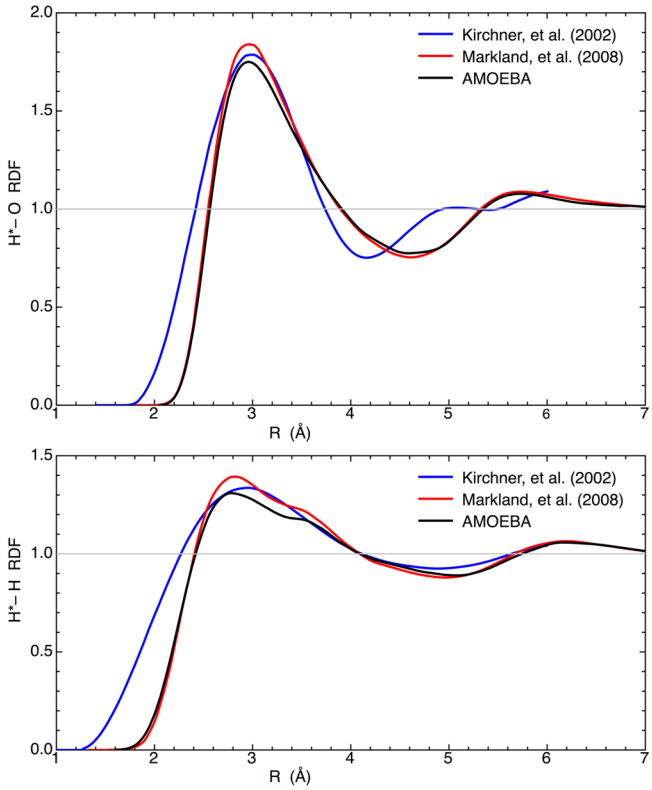

Figure 2. Radial distribution functions for H*−O and H*−H at ambient temperature.

To check the reliability of the BLYP method used in the Kirchner et al. study for energy evaluations, we carried out BLYP/aug-cc-pVTZ calculations for H* interacting with a single water molecule at the same geometries as in Figure 1, the results of which are shown in Figure S1 of the Supporting Information. Compared to the CCSD(T)/aug-cc-pVTZ benchmarks, the BLYP method is seen to have serious errors. Along most rays BLYP shows no attraction to water at all. The only exception to this is a minimum of about the correct magnitude for approach near a water H in the water plane at (90°, 45°), although even there the minimum occurs at too short distance. More seriously, for all approaches out of the water plane, as well as for approach in the plane at (90°, 45°), the repulsive wall occurs at significantly too short distance. This explains the anomalous behavior of the RDFs at short distances found in the Kirchner et al. study, and marks them as being unreliable.

The H*−O RDFs from the AMOEBA simulations at various temperatures are shown in the top panel of Figure 3. The position of the first maximum in the H*−O RDF remains essentially constant at 3.0 Å; the position of the first minimum varies slightly with temperature from 4.7 Å at 300 K to 4.3 Å at 646 K, and the position of the second maximum remains essentially constant with temperature at 5.8 Å. Overall the H*−O RDFs gradually flatten out with increasing temperature, so

dx.doi.org/10.1021/jp4106844 | J. Phys. Chem. B 2013, 117, 16530−16541

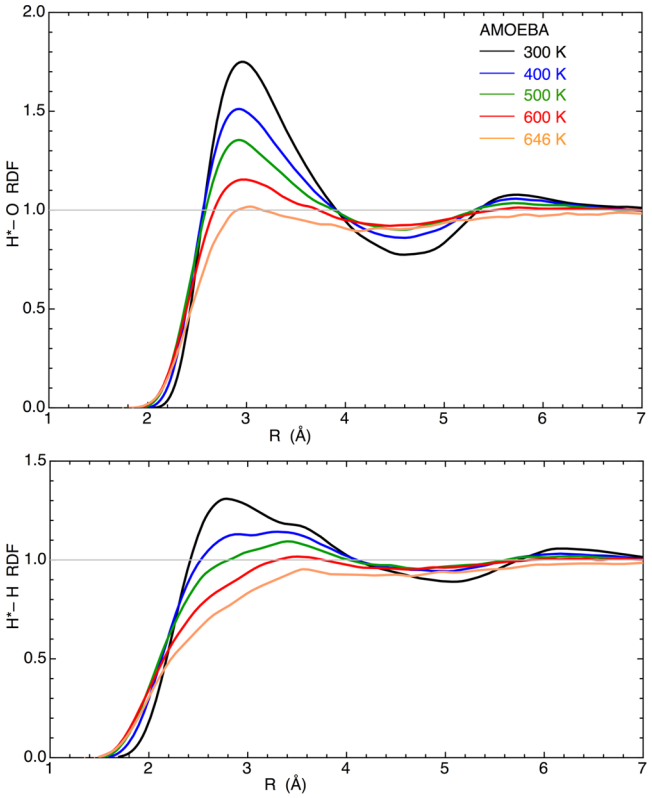

Figure 3. Radial distribution functions for H*−O and H*−H at different temperatures.

much that the second peak has essentially disappeared at the highest temperature considered.

The coordination number of H* can be defined as the number of water molecules whose H*−O distances are within the first minimum of the H*−O RDF. These values cannot be determined very precisely because they are quite sensitive to the exact positions of the first minima, which are not determined sufficiently precisely, especially at the higher temperatures. However, a rough determination can be made that the coordination numbers are about 13, 12, 10, 6, and 4 at the temperatures of 300, 400, 500, 600, and 646 K, respectively. Taking the first shell to start at about 2.0 Å, these coordination numbers correspond very approximately to densities of water molecules in the first solvation shell ranging from about 9% above the bulk water density at 300 K to about 13% below the bulk water density at 646 K.

The H*−H RDFs from the AMOEBA simulations at various temperatures are shown in the bottom panel of Figure 3. We start with discussion of the first peak at the lower temperatures of 300 and 400 K, where it has a bimodal structure. The position of the first maximum is at 2.8 Å, and a shoulder occurs at about 3.6 Å. Compared to the first maximum at 3.0 Å in the H*−O RDF, the H*−H RDF has its first maximum at 0.2 Å shorter and shoulder at 0.6 Å longer position. Thus, on average the first shell water molecules point one hydrogen slightly inward toward H* and the other significantly outward away from H* toward the second shell. The difference in the first maximum and shoulder of 0.8 Å is much shorter than the H−H distance of 1.55 Å in a water molecule, indicating that the outward pointing H is on average well out of the plane formed by H*, O, and the inward pointing H. These indications are consistent with an interpretation that the orientation of first shell water molecules is mainly determined by tendencies to donate one hydrogen bond to a second shell water molecule and to donate another hydrogen bond to a first shell water molecule.

At higher temperatures the bimodal structure of the first peak in the H*−H RDFs washes out. The first maximum at 2.8 Å disappears, and a new maximum appears at position slightly shorter than where the shoulder lies at lower temperatures. However, the peak retains its width, still having substantial amplitude where the first peak occurs at lower temperature. The discussion immediately above about water orientations in the first shell therefore probably remains qualitatively correct also at high temperatures. The position of the first minimum varies slightly with temperature from about 5.0 Å at 300 K to about 4.4 Å at 646 K, and the position of the second maximum remains essentially constant with temperature at 6.2 Å.

Angular Distribution Functions. Angular distribution functions (ADFs) were obtained to measure the disposition of H*−O−H angles χ for all waters in the first solvation shell. In principle we define this as the number of H*−O−H angles found between $\chi - d\chi/2$ and $\chi + d\chi/2$ divided by sin $\chi d\chi$ and renormalized such that the ADF times sin $\chi d\chi$ integrates to 2, the number of hydrogens in a water molecule. In practice we replace the infinitesimal width $d\chi$ by a finite bin size $\Delta\chi$ of 4°.

Results from the AMOEBA simulations at different temperatures are shown in Figure 4. The apparent irregularities seen

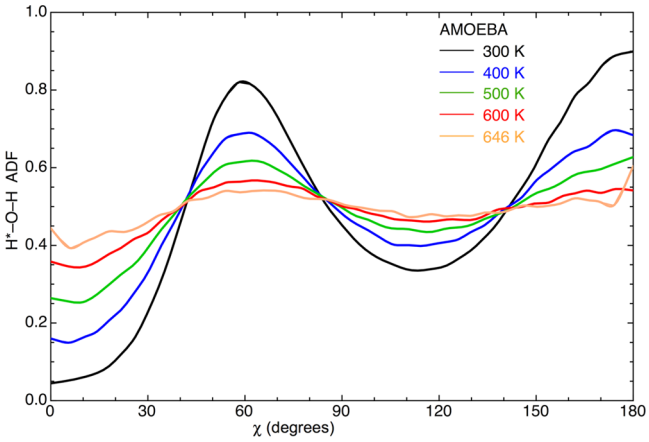

Figure 4. Angular distribution functions for H*−O−H at different temperatures.

for χ near 0° and 180° are artifacts due to the larger statistical uncertainties there, which become magnified upon dividing by the near-zero values of sin χ.

The qualitative shapes of the ADFs are similar at all temperatures, though the structures wash out more and more as temperature increases. The small values of the ADFs near 0° indicate that it is rare to have an OH bond point directly at or near H*. The maximum value of the H*−O−H average angle near 60° corresponds to one OH bond pointing slightly inward toward H*, and the other maximum value near 180° corresponds to the other OH bond pointing outward toward the second shell. This is fully consistent with the average orientations deduced above from examination of the RDFs. The maxima in the ADFs are separated by minima occurring near 115°, which is about midway between the maxima.

An important conclusion to be drawn from the RDFs and ADFs is that the first shell water molecules tend to orient

dx.doi.org/10.1021/jp4106844 | J. Phys. Chem. B 2013, 117, 16530−16541

themselves to avoid having any OH bonds directed toward H*, instead typically having one OH bond directed outward and the other OH bond oriented slightly inward. These observations are consistent with the first shell water molecules tending to donate one hydrogen bond to a second shell molecule and, to the extent possible, one hydrogen bond to another first-shell molecule. These tendencies are strongest near ambient temperatures, and decrease with temperature to remain only weakly true at the highest temperatures considered.

TRANSPORT

Diffusion. Diffusion can be characterized by computing the time evolution of the mean square displacement defined by

$$r^2(t) = \langle |r(t) - r(0)^2| \rangle$$

where the average is taken over many time origins. For long time intervals t Fickian diffusion pertains, and $r^2(t)$ becomes a linear function of t. The diffusion coefficient D is then given by the Einstein relation $D = r^2(t)/6t$. This was evaluated at each temperature from 10 trajectories of 1 ns duration each, dumping coordinates every 100 fs and averaging over all time origins separated by 1 ps. Statistical error was estimated to be the standard deviation from the mean of the individual x, y, and z components of the calculated diffusion coefficient. The time intervals t were considered within certain lower and upper limits. Since the Einstein relation is not valid at short times, intervals of less than 30 ps were excluded. An upper limit on t of 150 ps was imposed because the statistical errors were seen to deteriorate for longer times. Results were fitted to a simple activation model of $D = D_0 \exp(-E_a/RT)$.

Strictly speaking, the diffusion coefficient should more properly be evaluated in the microcanonical ensemble rather than the Berendsen weak coupling ensemble as presented here. However, it has been shown[50] that in practice the Berendsen weak coupling ensemble does produce essentially correct transport properties. We have also confirmed this in our previous study[24] of water self-diffusion with AMOEBA. To settle the matter beyond any reasonable doubt, we have also carried out trajectories of 2 ns for H* with 215 water molecules in the microcanonical ensemble, producing diffusion coefficients that agree with those presented here to within the estimated statistical error bars at all temperatures considered.

A reported experimental measurement[6] indicates the hydrogen atom diffusion coefficient in water is 0.77 ± 0.09 Å^2/ps at 298 K and has a temperature dependence over the range of 276−358 K that is governed by an activation energy E_a of 2.9 ± 0.4 kcal/mol. A previous classical MD study[14] reported a diffusion coefficient of 0.77 Å^2/ps at 315 K. A more recent study using ring polymer MD[16] at 298 K found classical and quantum values of 0.99 Å^2/ps and 0.93 Å^2/ps, respectively, indicating that quantum effects on the hydrogen nuclear motion decrease the diffusion coefficient by about 6% at ambient temperature. Quantum effects should rapidly become less important at higher temperatures.

Diffusion coefficients for the hydrogen atom from AMEOBA and from experiment are shown in Figure 5. The simulation results (shown in black) are seen to be in very close agreement with experiment (shown in blue) at near ambient temperatures, where comparison is possible. The simulation results were found to fit very well to a weighted linear regression of $\log(D)$ versus $1/T$ over the range of 300−575 K, while temperatures of 600 K and above were not included in the fit because of large

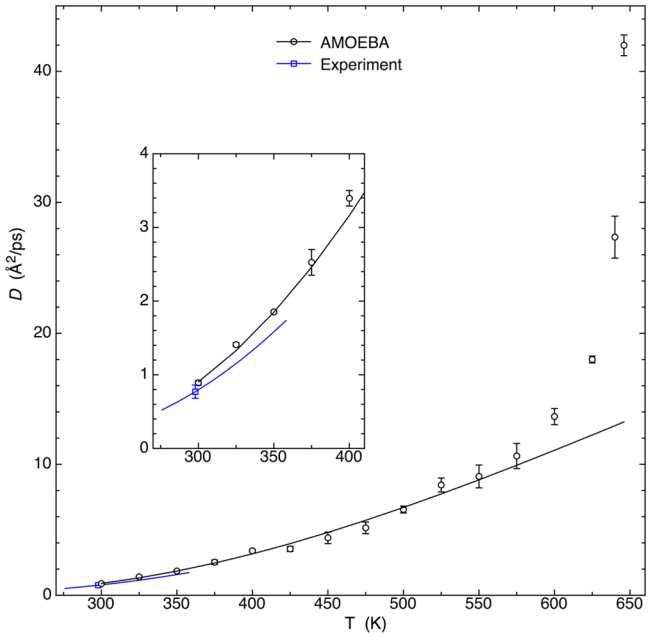

Figure 5. Calculated and experimental[6] results for hydrogen atom diffusion coefficient at various temperatures.

deviations from the fit. A slight extrapolation of the fit to 298 K produces a result of 0.88 Å^2/ps that is slightly above the given experimental range of 0.77 ± 0.09 Å^2/ps. Reduction of our computed result by 6% to account for quantum effects would produce a value of 0.83 Å^2/ps that is well within the given experimental range. The fit also produces an activation energy of 3.0 kcal/mol that is well within the given experimental range of 2.9 ± 0.4 kcal/mol. The curve resulting from fitting to the simulation results is also shown in Figure 5, where it is seen that the computed diffusion coefficients become significantly higher than the fit at temperatures of 600 K and above.

It may be concluded that the simulation gives hydrogen atom diffusion coefficients in good agreement with experiment at near-ambient temperatures, that the temperature dependence can be described by a simple activation model up to about 575 K, and that the diffusion becomes much faster than predicted by the simple activation model at very high temperatures.

Caging. It is of some interest to also consider the behavior of the mean square displacement over shorter time intervals. Three distinct regimes can be distinguished,[51] as follows.

For very short t the H* is usually between collisions with water molecules, and its motion is essentially ballistic, so $r^2(t) = \overline{v}^2 t^2$. Setting its average kinetic energy equal to the available thermal energy at 300 K leads to an average velocity $\overline{v}$ of 0.03 Å/fs. If the average distance traveled between collisions is on the order of 1−2 Å, then we estimate that the ballistic regime will last for a few tens of fs.

If there is significant trapping within nearly stationary cages before ultimate diffusion then there will be an intermediate t regime, known as dispersive transport, where $r^2(t)$ shows a sublinear growth as t^β with $\beta < 1$. This kind of behavior has been described with a continuous time random walk (CTRW) model[52−54] on a lattice wherein there is a wide range of waiting times between jumps, implying cages having a wide distribution of trap depths.

At very long t the transport will be dominated by Fickian diffusion, and $r^2(t)$ will grow linearly with t. On the basis of the

dx.doi.org/10.1021/jp4106844 | J. Phys. Chem. B 2013, 117, 16530−16541

discussion in the previous subsection, this latter regime will be on the order of tens of ps and longer.

Since these three different time regimes vary over several orders of magnitude, they are best distinguished on a logarithmic scale. Thus, the expectation is that a log−log plot of $r^2(t)$ versus t will show a slope of about 2 in the ballistic regime of very short t, a slope β of less than 1 if there is significant caging in the regime of intermediate t, and a slope of nearly 1 in the Fickian diffusion regime of very long t.[51]

To test these predictions, two of the 1 ns trajectories at several temperatures were run with more frequent dumping of coordinates every fs and averaged over all time origins separated by 1 fs.

The results at 300 K are shown in the left panel of Figure 6. The solid line shows values of $r^2(t)$ obtained from the

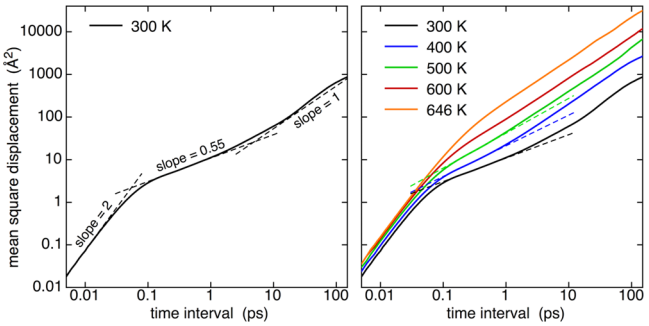

Figure 6. Mean square displacement $r^2(t)$ vs time interval t on a log−log scale.

simulation. The leftmost dashed line with slope 2 shows the expectation at very short times of $r^2(t) = \bar{v}^2t^2$, with $\bar{v}$ obtained by setting the H* kinetic energy equal to the thermal energy. The fit is seen to be excellent, confirming ballistic motion at very short times up to ∼30 fs, which is in good accord with the estimate made above of the extent of the ballistic regime. The rightmost dashed line with slope 1 shows the expectation at very long times of $r^2(t) = 6Dt$ with diffusion constant D as determined in the subsection above. This fit is good, although less than perfect because the statistics of the two 1 ns runs used for this demonstration are poorer than those from the 10 ns used to determine D. This confirms the Fickian diffusion at times longer than ∼20 ps.

The particularly interesting point to notice about the left panel of Figure 6 is that the slope does not pass monotonically from 2 to 1. There is an intermediate regime of t from ∼0.1 to 1 ps, where a straight line fit shown with the center dashed line has slope β of 0.55. This small slope of less than unity clearly indicates that some caging behavior pertains in this time regime, along with some net translational motion as well.

Apparently the cages are very dynamic and only impede the diffusion of H* for at most a few ps. This time scale is on the order of librational motions of water and is much shorter than diffusional motion of water. This is consisent with an interpretation that the H* remains in a cage until some collective librational motion of the nearby water molecules opens a gate allowing the H* to pass to an adjacent nascent cage.

The right panel of Figure 6 shows the values of $r^2(t)$ obtained from the simulation at various temperatures. Although not shown for reasons of clarity, the very short time and very long time behaviors fit well at each temperature to those expected from ballistic and Fickian behavior, respectively. The intermediate time regime shows evidence of caging at all but the highest temperatures, with slopes of the dashed lines shown of 0.55, 0.72, and 0.82 at 300, 400, and 500 K, respectively. At 600 K the statistics are not good enough to determine whether or not there may be a caging regime with slope slightly less than 1. At 646 K there is no evidence of caging at all, as the slope passes smoothly from 2 to 1 with increasing t. It is concluded that up to temperatures of at least 500 K there exists a caging regime extending to about 1 ps .

Experimental measurements of the hydrogen atom hyperfine coupling constant[17,18] have been interpreted with a model that envisions the H* to be vibrating inside a spherical cage with a characteristic frequency arising from a radial harmonic potential. However, examination of the Fourier transforms of our mean square displacements does not show any evidence of a particular vibrational frequency. Thus, we confirm the notion of caging but not of any characteristic vibrational motions within the cages.

HYPERFINE COUPLING

Hyperfine Coupling in Vacuum. The observed effect of hydration on A/A_{vac} is small, less than 1%, so it is wise to first investigate the accuracy of those assumptions commonly made to compute A.

The hyperfine coupling constant for an electron interacting with a nucleus N of nonzero spin is usually calculated from the Fermi contact interaction using the standard expression

$$A = \frac{8\pi}{3} g_e \beta_e g_N \beta_N [\rho_\alpha(0) - \rho_\beta(0)]$$

where g_e is the electron g-factor, $\beta_e = e\hbar/2m_ec$ is the Bohr magneton, g_N is the g-factor of the nucleus, $\beta_N = e\hbar/2m_Nc$ is the nuclear magneton, and $\rho_\alpha(0) - \rho_\beta(0)$ is the electron spin density evaluated at the nucleus.

For the hydrogen atom in vacuum, using the exact nonrelativistic hydrogen atom wave function with treatment of the nucleus as a clamped point particle, one obtains the spin density at the nucleus as $1/\pi a_0^3$. Adopting the usual Bohr radius of $a_0 = \hbar^2/m_ee^2$, along with modern values of the requisite physical constants,[55] leads to the value of A = 1422.81 MHz for the hydrogen atom in vacuum, which has an error of 0.17% when compared to the experimental value[56] of 1420.41 MHz. Most of this error is removed by accounting for the finite mass of the nucleus[57] through replacing a_0 with a reduced Bohr radius of $a_0' = \hbar^2/\mu_ee^2$, where $\mu_e = m_em_N/(m_e + m_N)$ is the electron−hydrogen reduced mass, to produce a spin density at the nucleus of $1/\pi a_0'^3$. This replacement leads to the value of A = 1420.49 MHz, having an error of only 0.006% when compared to the experimental value. The remaining slight discrepancy, which arises from several sources, including the finite size and charge distribution of the nucleus, relativistic corrections, and quantum electrodynamic effects,[57] is negligible for the present purposes. It is concluded that adoption of the Fermi contact expression with spin density obtained from nonrelativistic electronic structure methods invoking point nuclei is quite adequate here for calculation of A.

We next consider suitable basis sets for benchmark hyperfine coupling calculations. Approximating the hydrogen atom wave function in vacuum with the aug-cc-pVTZ basis set[40,41] leads to a spin density at the nucleus of 0.2870 au, in error by 9.82% from the exact value of $1/\pi$ = 0.3183 au. This can be greatly improved by supplementing the basis with four additional tight

dx.doi.org/10.1021/jp4106844 | J. Phys. Chem. B 2013, 117, 16530−16541

s-functions at hydrogen to refine the behavior near the nucleus. The exponents of the additional tight *s*-functions are chosen to follow a geometric progression from the existing innermost exponents. This yields a basis set designated here as supp-aug-cc-pVTZ having spin density at the nucleus of 0.3189 au, corresponding to an error of only 0.19% from the exact value. Assuming that this remaining small error will be largely consistent and so effectively cancel out in taking the ratio A/A_{vac}, we use the supp-aug-cc-pVTZ basis set for benchmark purposes in the following subsection.

Protocol for Hyperfine Coupling Calculations. For a hydrogen atom in the condensed phase, the value of g_e will differ from the free electron value. However, measurements on g_e of the hydrogen atom in water[18] show that it differs from the free-electron value by less than 60 ppm over a wide range of temperatures. This is a negligible difference for the present purposes, so we simply use the free-electron value of g_e in our calculations of A. Most of the factors involved in the Fermi contact expression, including g_e and the a_0 in the spin density, then actually drop out in taking the ratio of A/A_{vac} for the hydrogen atom.

We eventually wish to calculate A/A_{vac} for a large collection of clusters extracted from MD snapshots, each cluster containing many water molecules surrounding H*. This demanding program requires identification of an electronic structure method that is highly efficient and yet sufficiently accurate. We start the search by first considering calculations on H* interacting with one or two water molecules, where high-level benchmark calculations can be made for comparison. The benchmark results are obtained from CCSD/supp-aug-cc-pVTZ calculations using relaxed coupled cluster densities. We note that the presence of polarization functions in the nucleus-centered basis set allows the wave function in the vicinity of H* to be distorted by the presence of nearby water and thereby effectively describes any possible shift of the center of charge of the H* electron away from the H* nucleus.

The third and sixth rows of Figure 1 show in black the benchmark results for A/A_{vac} of H* interacting with one water molecule along each of the eleven symmetry-unique rays. To limit consideration to the most physically significant regions of interaction energies, the lower and upper limits on distance shown in each plot are taken to be the same as those determined for the energy calculations that are shown in the second and fifth rows. The typical behavior of the benchmark results is that A/A_{vac} is essentially unity at large distance, while as distance decreases A/A_{vac} gradually increases up to some maximum value above unity, after which it ultimately drops off sharply to values below unity at short distance. Along some of the rays this maximum and utlimate drop off is not yet achieved before the plot is cut off because of the interaction energy becoming very repulsive.

It turns out in hindsight that the supp-aug-cc-pVTZ is overkill for this purpose. Even though the aug-cc-pVTZ basis set gives a signficant error for A_{vac} itself, CCSD calculations of A/A_{vac} using the aug-cc-pVTZ basis differ from those using the supp-aug-cc-pVTZ basis by less than 0.04% at all the points used in the benchmark studies described just above. Thus, the errors in using the aug-cc-pVTZ basis set for hyperfine coupling calculations are also largely consistent and effectively cancel out in taking the ratio A/A_{vac}.

To identify a more efficient means to evaluate the hyperfine coupling, we have examined many of the commonly used density functional theory (DFT) approaches without finding any that satisfactorily mimic the benchmark CCSD/aug-cc-pVTZ results. However, after considerable experimentation it was found that a hybrid functional that we denote as PBE40 performs well. The PBE40 functional modifies the original PBE exchange-correlation functional[58] to become a hybrid composed of the PBE correlation functional, 40% of the PBE exchange functional, and 60% of exact exchange. The third and sixth rows of Figure 1 show in blue results for A/A_{vac} from the PBE40 method as implemented with a mixed basis set of aug-cc-pVTZ on H* and 6-31+G*[59−61] on water. The agreement with the benchmark values is generally quite good.

The hyperfine coupling results in Figure 1 document the performance of PBE40/aug-cc-pVTZ;6-31+G* in reproducing benchmark CCSD/aug-cc-pVTZ results only for two-body effects on A/A_{vac}. It is of interest to also check on how well it describes three-body effects. As with the check on three-body interaction energies, we inspected the same 100 random snapshots from the 300 K simulation and extracted from each snapshot the coordinates of H* along with the closest two water molecules for analysis. The benchmark three-body effects on A/A_{vac} from CCSD/aug-cc-pVTZ ranged from −0.0033 to +0.0047, which is quite significant, being of the same magnitude as the effects being investigated. The analogous three-body effects from PBE40/aug-cc-pVTZ;6-31+G* agreed with those from the benchmarks with a mean unsigned error of just 0.0004. Since this analysis used the most challenging cases of the closest water molecules, the significant three-body effects on A/A_{vac} seem to be quite satisfactorily described in general by the PBE40/aug-cc-pVTZ;6-31+G* method.

It is concluded that the PBE40/aug-cc-pVTZ;6-31+G* method should be suitable for the evaluation of A/A_{vac} in large clusters. Still, it is useful to investigate where the most significant errors may lie. Upon scrutinizing the two-body calculations more closely, the PBE40/aug-cc-pVTZ;6-31+G* method is seen to typically give A/A_{vac} results very close to or just slightly higher than the benchmarks at large to intermediate values of R and then to fall somewhat below the benchmarks at very short values of R.

The next step in the development of a computational protocol is to establish how many water molecules must be explicitly treated in clusters to reliably determine the effect of bulk water on A/A_{vac}. This exercise was done at the DFT level with the PBE40/aug-cc-pVTZ;6-31+G* method, using temperatures of 300 and 600 K to represent the full range of temperatures considered. The smallest collection considered included all water molecules having O atoms within 4.6 Å of H*, which is about the extent of the first solvation shell, which on average includes 13 waters at 300 K to about 6 waters at 600 K. A larger collection included all water molecules having O atoms within 6.5 Å of H*, which on average includes 29 waters at 300 K to about 18 waters at 600 K. The largest collection included all water molecules having O atoms within 7.0 Å of H*, which on average includes 47 waters at 300 K to about 30 waters at 600 K

At each temperature 1000 snapshots of the MD simulation were collected in 1 ps increments for analysis. At 300 K the averaged value of A/A_{vac} changed slightly with the cluster size, being 1.00808, 1.00943, and 1.00953 for inclusion of all waters within 4.6, 6.5, and 7.0 Å of H*, respectively. At 600 K the dependence on cluster size was even less; the averaged values of A/A_{vac} were 1.00189, 1.00192, and 1.00190 for those same size criteria. Including all waters within 4.6 Å of H* is enough for semiquantitative evaluation of A/A_{vac}, and including all waters

dx.doi.org/10.1021/jp4106844 | J. Phys. Chem. B 2013, 117, 16530−16541

within 6.5 Å of H* is sufficient for quantitative evaluation of the effect of bulk water on A/A_{vac}.

Aqueous Hyperfine Coupling Results. For the final hyperfine results, 1000 snapshots collected in 1 ps increments were analyzed at each temperature. A cluster containing H* and all water molecules within 6.5 Å was extracted from each snapshot and used to compute A/A_{vac} with the PBE40/aug-cc-pVTZ;6-31+G* method. The results for A/A_{vac} after averaging over all clusters are shown as a function of temperature in the top panel of Figure 7. Statistical error bars obtained as the

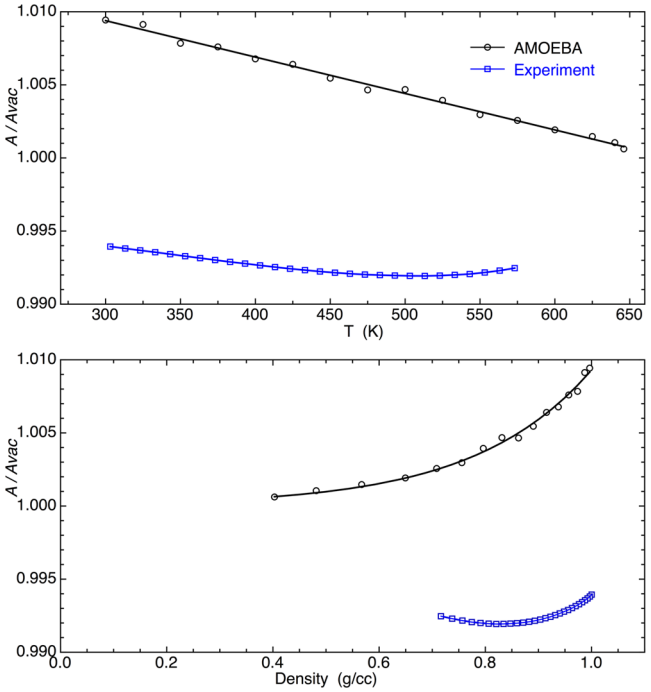

Figure 7. Calculated and experimental[17,18] results for A/A_{vac} of aqueous H* at various temperatures (top panel) or at various densities (bottom panel).

standard deviation from the mean of all snapshots are about the same size as the symbols and so are not shown. The computational results display a nearly linear decrease in A/A_{vac} with temperature, from 1.0094 at 300 K to 1.0006 at 646 K. A linear regression fit yields $A/A_{vac} = 1.0094 - 2.5 \times 10^{-5}\ (T - 300\ \text{K})$.

Experimental results are also included in the top panel of Figure 7 for comparison. These were obtained for temperatures ranging from 303 to 573 K at fixed pressure of 105 bar. The A/A_{vac} results range from 0.9939 at 303 K to a minimum of 0.9918 at 513 K and then rise somewhat at still higher temperatures. At the lower temperatures the decrease is nearly linear with temperature. A linear regression fit over the temperature range 303−403 K yields $A/A_{vac} = 0.9940 - 1.3 \times 10^{-5}\ (T - 300\ \text{K})$.

Strictly speaking the AMOEBA and experimental results for A/A_{vac} in the top panel of Figure 7 should not be directly compared with one another because at each temperature they correspond to different densities. The AMOEBA result at each temperature was obtained at the density corresponding to the liquid−vapor coexistence curve of neat water, whereas the experimental result was obtained at the density corresponding to fixed pressure of 105 bar. For comparison of AMOEBA to experimental results it is more appropriate to plot A/A_{vac} against density, as shown in the bottom panel of Figure 7. This plot also facilitates judgment of the approach to gas phase behavior in the limit of low density. The black line shows a smoothed curve to guide the eye through the AMOEBA results that indicate a gradual approach to unity from above at very low densities, while the experimental results appear to gradually approach unity from below.

The agreement of the calculations with experiment is clearly not good. The only qualitative point of agreement is the finding that A/A_{vac} decreases nearly linearly with temperature at the lower temperatures considered. However, the actual values are quite different, with A/A_{vac} being consistently above unity in the calculations, while the experiments give A/A_{vac} below unity throughout. Furthermore, the slope of the linear regime is 1.9 times higher in magnitude in the calculation than it is in the experiment. Finally, the experiment shows a minimum and subsequent increase of A/A_{vac} at high temperatures, whereas the calculations still persist in maintaining a near-linear decrease.

By comparing to benchmark results, it is possible to estimate how much the calculated A/A_{vac} values might change if the MD simulations were carried out with a more accurate force field and the hyperfine coupling constants were evaluated with a more accurate electronic structure method. For this purpose, assume that the deviation from unity of A/A_{vac} will be dominated by the influence of first-shell water molecules on H*. From the discussion above on RDFs and ADFs it was found that these are typically oriented such that H* is out of the water plane and away from the water hydrogens, such as for the configurations in the bottom half of Figure 1. At low temperatures the AMOEBA force field often allows the H* to approach a little too close to water over a distance range where the PBE40/aug-cc-pVTZ;6-31+G* method gives values of A/A_{vac} that, at typical orientations, range from about 0.0010 above or below the benchmark values. Therefore the PBE40/aug-cc-pVTZ;6-31+G* error in A/A_{vac} at low temperatures should be small, probably somewhat less than 0.0010, and might be of either sign. At high temperatures the AMOEBA force field often keeps the H* a little too far away from water over a distance range where the PBE40/aug-cc-pVTZ;6-31+G* method gives values of A/A_{vac} that, at typical orientations, range from about 0.0010 to 0.0070 below the benchmark values. Therefore the PBE40/aug-cc-pVTZ;6-31+G* error in A/A_{vac} at high temperatures may be significant in the direction of being too low, which is the wrong direction to improve agreement with experiment.

The cause of these disagreements between calculated and experimental values of A/A_{vac} is not clear at this time. One possibility is that the classical treatment of trajectories is not adequate. A quantum treatment of the H* nuclear motion would allow it to penetrate into the classically forbidden region close to a water molecule, thereby increasing the sampling of regions where the hyperfine coupling constant is below unity. Clearly more research on this system is needed, and we leave the issue here as an unresolved matter at this time.

CONCLUSION

This work reports computational studies of a hydrogen atom H* in water from ambient temperature to near the critical point of water. MD simulations are carried out to determine structural and diffusion properties, and electronic structure calculations are used to determine hyperfine coupling constants.

dx.doi.org/10.1021/jp4106844 | J. Phys. Chem. B 2013, 117, 16530−16541

A force field of AMOEBA form for use in MD simulations is obtained by fitting to high level electronic structure calculations on H* interacting with one water molecule. The fit of two body interactions is found to be satisfactory at all angles of approach and very good for H* approaching W laterally in the plane. Although not considered during the fitting, the effects of three-body interactions are found to be small and represented reasonably well by virtue of including polarizability in the force field.

The MD simulations at ambient temperature produce RDFs in very good agreement with one previous literature report[16] but poor agreement with another previous literature report.[14] The latter disagreement is attributed to use in the literature work of the BLYP functional for energy evaluations, which gives a poor description of the correct two-body interactions. In our work the H*−O RDFs show first minima ranging from 4.7 Å at 300 K to 4.3 Å at 646 K, from which coordination numbers ranging from about 13 to about 4 are determined. The RDFs and ADFs indicate that first-shell water molecules rarely point an OH bond directly toward H*, instead typically pointing one OH bond outward toward the second shell and the remaining OH bond orienting slightly inward but mainly pointing toward another first shell water molecule, these presumably to maximize hydrogen bonding to the extent possible. These orientational tendencies are strongest near ambient temperatures and decrease with temperature to remain only weakly true at the highest temperatures considered.

The diffusion coefficient is calculated to be in good agreement with experiment at ambient temperature and in good agreement with the experimental temperature dependence near there. The calculations at various temperatures produce diffusion coefficients that can be fitted very well with a simple activation model up to about 575 K, while the diffusion becomes much faster than predicted by the simple activation model at higher temperatures. Up to temperatures of at least 500 K there is clear evidence for caging on a time scale of about 1 ps, but the evidence disappears at the highest temperatures considered.

A DFT method constructed as a PBE40 hybrid is found that gives hyperfine coupling constants for H* interacting with a water molecule that are in good agreement with high level electronic structure calculations. Three-body effects on the hyperfine coupling constant are found to be both significant and reasonably well described by the DFT method. Calculations on clusters containing H* surrounded by all water molecules within 6.5 Å are sufficient to mimic the effect of bulk water on the hyperfine coupling. Values of A/A_{vac} are obtained by averaging the results of DFT calculations on such clusters extracted from snapshots of the MD simulations at each temperature. The results do not agree well with experiment, giving values of A/A_{vac} consistently above unity, while the experiment gives values below unity throughout. Although the calculations qualitatively agree with experiment in showing a near-linear decrease in A/A_{vac} at low temperatures, the calculations show a rate of decrease nearly twice that reported in the experiment. Also, the calculations show the decrease to continue at very high temperatures, while the experimental report exhibits a minimum and then an increase in A/A_{vac} at high temperatures. The source of these discrepancies on the hyperfine coupling behavior is not understood at present, pointing to the need for further research on this problem.

■ ASSOCIATED CONTENT

Supporting Information

Figure S1 shows geometries for the H−W interaction and interaction energies. This material is available free of charge via the Internet at http://pubs.acs.org.

■ AUTHOR INFORMATION

Corresponding Author

*E-mail: chipman.1@nd.edu.

Present Address

[§]A.P. Inorganic Chemistry Group, Department of Chemistry, St. Petersburg State University, University Pr. 26, Old Peterhof, 198504, Russia

Notes

The authors declare no competing financial interest.

■ ACKNOWLEDGMENTS

Helpful conversations with D. Bartels, K. Nuzhdin, I. Carmichael, J. D. Gezelter, and J. Sapirstein are gratefully acknowledged. The research described herein was supported by the Division of Chemical Sciences, Geosciences and Biosciences, Basic Energy Sciences, Office of Science, United States Department of Energy through Grant number DE-FC02-04ER15533. This is contribution number NDRL 4989 from the Notre Dame Radiation Laboratory.

■ REFERENCES

(1) Spinks, J. W. T.; Woods, R. J. *An Introduction to Radiation Chemistry*, 3rd ed.; Wiley-Interscience: New York, 1990.

(2) Garrett, B. C.; Dixon, D. A.; Camaioni, D. M.; Chipman, D. M.; Johnson, M. A.; Jonah, C. D.; Kimmel, G. A.; Miller, J. H.; Rescigno, T. N.; Rossky, P. J.; et al. Role of Water in Electron-Initiated Processes and Radical Chemistry: Issues and Scientific Advances. *Chem. Rev.* **2005**, *105*, 355−389.

(3) Mozumder, A. Ionization and Excitation Yields in Liquid Water due to the Primary Irradiation: Relationship of Radiolysis with Far UV-Photolysis. *Phys. Chem. Chem. Phys.* **2002**, *4*, 1451−1456.

(4) Janik, D.; Janik, I.; Bartels, D. M. Neutron and beta/gamma Radiolysis of Water up to Supercritical Conditions. 1. beta/gamma Yields for H2, H. Atom, and Hydrated Electron. *J. Phys. Chem. A* **2007**, *111*, 7777−7786.

(5) Elliot, A. J.; Bartels, D. M. *The Reaction Set, Rate Constants and g-Values for the Simulation of the Radiolysis of Light Water over the Range 20° to 350°C Based on Information Available in 2008*; Atomic Energy of Canada, Ltd.: Ontario, Canada, 2009.

(6) Benderskii, V. A.; Krivenko, A. G. Diffusion of Hydrogen and Deuterium Atoms in Water. *Russ. J. Electrochem.* **1996**, *32*, 663−669.

(7) Mills, R. Self-Diffusion in Normal and Heavy Water in the Range 1−45 Degrees. *J. Phys. Chem.* **1973**, *77*, 685−688.

(8) Lee, S. H.; Rasaiah, J. C. Proton Transfer and the Mobilities of the H+ and OH- Ions from Studies of a Dissociating Model for Water. *J. Chem. Phys.* **2011**, *135*, 124505:1−10.

(9) Eiben, K.; Fessenden, R. W. Electron Spin Resonance Studies of Transient Radicals in Aqueous Solutions. *J. Phys. Chem.* **1971**, *75*, 1186−1201.

(10) Fessenden, R. W.; Hornak, J. P.; Venkataraman, B. Electron Spin-Lattice Relaxation Times of Transient Free Radicals. *J. Chem. Phys.* **1981**, *74*, 3694−3704.

(11) Tse, J. S.; Klein, M. L. Are Hydrogen Atoms Solvated by Water Molecules? *J. Phys. Chem.* **1983**, *87*, 5055−5057.

(12) De Raedt, B.; Sprik, M.; Klein, M. L. Computer Simulation of Muonium in Water. *J. Chem. Phys.* **1984**, *80*, 5719−5724.

(13) Gai, H. D.; Garrett, B. C. Path Integral Calculations of the Free Energies of Hydration of Hydrogen Isotopes (H, D, and Mu). *J. Phys. Chem.* **1994**, *98*, 9642−9648.

(14) Kirchner, B.; Stubbs, J.; Marx, D. Fast Anomalous Diffusion of Small Hydrophobic Species in Water. *Phys. Rev. Lett.* **2002**, *89*, 215901:1−4.
(15) Renault, J. P.; Vuilleumier, R.; Pommeret, S. Hydrated Electron Production by Reaction of Hydrogen Atoms with Hydroxide Ions: A First-Principles Molecular Dynamics Study. *J. Phys. Chem. A* **2008**, *112*, 7027−7034.
(16) Markland, T. E.; Habershon, S.; Manolopoulos, D. E. Quantum Diffusion of Hydrogen and Muonium Atoms in Liquid Water and Hexagonal Ice. *J. Chem. Phys.* **2008**, *128*, 194506:1−11.
(17) Roduner, E.; Percival, P. W.; Han, P.; Bartels, D. M. Isotope and Temperature Effects on the Hyperfine Interaction of Atomic Hydrogen in Liquid Water and in Ice. *J. Chem. Phys.* **1995**, *102*, 5989−5997.
(18) Nuzhdin, K.; Bartels, D. M. Hyperfine Coupling of the Hydrogen Atom in High Temperature Water. *J. Chem. Phys.* **2013**, *138*, 124503:1−8.
(19) Ponder, J. W. *TINKER: Software Tools for Molecular Design, Version 4.2.*; Washington University School of Medicine: Saint Louis, MO, 2004.
(20) Shao, Y.; Molnar, L. F.; Jung, Y.; Kussmann, J.; Ochsenfeld, C.; Brown, S. T.; Gilbert, A. T. B.; Slipchenko, L. V.; Levchenko, S. V.; O'Neill, D. P.; et al. Advances in Methods and Algorithms in a Modern Quantum Chemistry Program Package. *Phys. Chem. Chem. Phys.* **2006**, *8*, 3172−3191.
(21) Ren, P.; Ponder, J. W. Polarizable Atomic Multipole Water Model for Molecular Mechanics Simulation. *J. Phys. Chem. B* **2003**, *107*, 5933−5947.
(22) Ren, P.; Ponder, J. W. Temperature and Pressure Dependence of the AMOEBA Water Model. *J. Phys. Chem. B* **2004**, *108*, 13427−13437.
(23) Wang, L.-P.; Head-Gordon, T.; Ponder, J. W.; Ren, P.; Chodera, J. D.; Eastman, P. K.; Martinez, T. J.; Pande, V. S. Systematic Improvement of a Classical Molecular Model of Water. *J. Phys. Chem. B* **2013**, *117*, 9956−9972.
(24) Chipman, D. M. Water from Ambient to Supercritical Conditions with the AMOEBA Model. *J. Phys. Chem. B* **2013**, *117*, 5148−5155.
(25) Ponder, J. W.; Wu, C.; Ren, P.; Pande, V. S.; Chodera, J. D.; Schnieders, M. J.; Haque, I.; Mobley, D. L.; Lambrecht, D. S.; DiStasio, R. A., Jr.; et al. Current Status of the AMOEBA Polarizable Force Field. *J. Phys. Chem. B* **2010**, *114*, 2549−2564.
(26) Ren, P.; Wu, C.; Ponder, J. W. Polarizable Atomic Multipole-Based Molecular Mechanics for Organic Molecules. *J. Chem. Theory Comput.* **2011**, *7*, 3143−3161.
(27) Shi, Y.; Wu, C.; Ponder, J. W.; Ren, P. Multipole Electrostatics in Hydration Free Energy Calculations. *J. Comput. Chem.* **2011**, *32*, 967−977.
(28) Grossfield, A.; Ren, P.; Ponder, J. W. Ion Solvation Thermodynamics from Simulation with a Polarizable Force Field. *J. Am. Chem. Soc.* **2003**, *125*, 15671−15682.
(29) Grossfield, A. Dependence of Ion Hydration on the Sign of the Ion's Charge. *J. Chem. Phys.* **2005**, *122*, 024506:1−10.
(30) Jiao, D.; King, C.; Grossfield, A.; Darden, T. A.; Ren, P. Simulation of Ca^{2+} and Mg^{2+} Solvation using Polarizable Atomic Multipole Potential. *J. Phys. Chem. B* **2006**, *110*, 18553−18559.
(31) Piquemal, J.-P.; Perera, L.; Cisneros, G. A.; Ren, P.; Pedersen, L. G.; Darden, T. A. Towards Accurate Solvation Dynamics of Divalent Cations in Water using the Polarizable Amoeba Force Field: From Energetics to Structure. *J. Chem. Phys.* **2006**, *125*, 054511:1−7.
(32) Rogers, D. M.; Beck, T. L. Quasichemical and Structural Analysis of Polarizable Anion Hydration. *J. Chem. Phys.* **2010**, *132*, 014505:1−12.
(33) Wu, J. C.; Piquemal, J.-P.; Chaudret, R.; Reinhardt, P.; Ren, P. Polarizable Molecular Dynamics Simulation of Zn(II) in Water Using the AMOEBA Force Field. *J. Chem. Theory Comput.* **2010**, *6*, 2059−2070.
(34) Zhao, Z.; Rogers, D. M.; Beck, T. L. Polarization and Charge Transfer in the Hydration of Chloride Ions. *J. Chem. Phys.* **2010**, *132*, 014502:1−10.
(35) Thole, B. T. Molecular Polarizabilities Calculated with a Modified Dipole Interaction. *Chem. Phys.* **1981**, *59*, 341−350.
(36) Halgren, T. A. Representation of van der Waals (vdW) Interactions in Molecular Mechanics Force Fields: Potential Form, Combination Rules, and vdW Parameters. *J. Am. Chem. Soc.* **1992**, *114*, 7827−7843.
(37) Pauling, L.; Wilson, E. B., Jr. *Introduction to Quantum Mechanics*; McGraw-Hill: New York, 1935.
(38) Purvis, G. D.; Bartlett, R. J. A Full Coupled-Cluster Singles and Doubles Model: The Inclusion of Disconnected Triples. *J. Chem. Phys.* **1982**, *76*, 1910−1918.
(39) Raghavachari, K.; Trucks, G. W.; Pople, J. A.; Head-Gordon, M. A Fifth-Order Comparison of Electron Correlation Theories. *Chem. Phys. Lett.* **1989**, *157*, 479−483.
(40) Dunning, T. H., Jr. Gaussian Basis Sets for use in Correlated Molecular Calculations. I. The Atoms Boron Through Neon and Hydrogen. *J. Chem. Phys.* **1989**, *90*, 1007−1023.
(41) Kendall, R. A.; Dunning, T. H., Jr.; Harrison, R. J. Electron Affinities of the First-Row Atoms Revisited. Systematic Basis Sets and Wave Functions. *J. Chem. Phys.* **1992**, *96*, 6796−6806.
(42) Boys, S. F.; Bernardi, F. The Calculation of Small Molecular Interactions by the Differences of Separate Total Energies. Some Procedures with Reduced Errors. *Mol. Phys.* **1970**, *19*, 553−566.
(43) Alexandrova, A. N. H(H2O)(n) Clusters: Microsolvation of the Hydrogen Atom via Molecular ab Initio Gradient Embedded Genetic Algorithm (GEGA). *J. Phys. Chem. A* **2010**, *114*, 12591−12599.
(44) Medders, G. R.; Babin, V.; Paesani, F. A Critical Assessment of Two-Body and Three-Body Interactions in Water. *J. Chem. Theory Comput.* **2013**, *9*, 1103−1114.
(45) Berendsen, H. J. C.; Postma, J. P. M.; van Gunsteren, W. F.; Dinola, A.; Haak, J. R. Molecular Dynamics with Coupling to an External Bath. *J. Chem. Phys.* **1984**, *81*, 3684−3690.
(46) Morishita, T. Fluctuation Formulas in Molecular-Dynamics Simulations with the Weak Coupling Heat Bath. *J. Chem. Phys.* **2000**, *113*, 2976−2982.
(47) Beeman, D. Some Multistep Methods for use in Molecular Dynamics Calculations. *J. Comp Phys.* **1976**, *20*, 130−139.
(48) Brooks, B. R. *Algorithms for Molecular Dynamics at Constant Temperature and Pressure*. National Institutes of Health: Bethesda, MD, 1988.
(49) Bartels, D. M.; Han, P.; Percival, P. W. Diffusion and CIDEP of H and D Atoms in Solid H2O, D2O and Isotopic Mixtures. *Chem. Phys.* **1992**, *164*, 421−437.
(50) Basconi, J. E.; Shirts, M. R. Effects of Temperature Control Algorithms on Transport Properties and Kinetics in Molecular Dynamics Simulations. *J. Chem. Theory Comput.* **2013**, *9*, 2887−2899.
(51) Kob, W.; Andersen, H. C. Testing Mode-Coupling Theory for a Supercooled Binary Lennard-Jones Mixture: The van Hove Correlation Function. *Phys. Rev. E: Stat., Nonlinear, Soft Matter Phys.* **1995**, *51*, 4626−4641.
(52) Klafter, J.; Zumofen, G. Probability Distributions for Continuous-Time Random Walks with Long Tails. *J. Phys. Chem.* **1994**, *98*, 7366−7370.
(53) Shlesinger, M. F.; Klafter, J.; Zumofen, G. Above, Below and Beyond Brownian Motion. *Am. J. Phys.* **1999**, *67*, 1253−1259.
(54) Vardeman, C. F.; Gezelter, J. D. Comparing Models for Diffusion in Supercooled Liquids: The Eutectic Composition of the Ag-Cu Alloy. *J. Phys. Chem. A* **2001**, *105*, 2568−2574.
(55) Mohr, P. J.; Taylor, B. N.; Newell, D. B. CODATA Recommended Values of the Fundamental Physical Constants: 2010. *Rev. Mod. Phys.* **2012**, *84*, 1527−1605.
(56) Essen, L.; Donaldson, R. W.; Hope, E. G.; Bangham, M. Hydrogen Maser Work at the National Physical Laboratory. *Metrologia* **1973**, *9*, 128−137.

(57) Karshenboim, S. G. Precision Physics of Simple Atoms: QED Tests, Nuclear Structure and Fundamental Constants. *Phys. Rep.* **2005**, *422*, 1−63.
(58) Adamo, C.; Scuseria, G. E.; Barone, V. Accurate Excitation Energies from Time-Dependent Density Functional Theory: Assessing the PBE0 Model. *J. Chem. Phys.* **1999**, *111*, 2889−2899.
(59) Hehre, W. J.; Ditchfield, R.; Pople, J. A. Self-Consistent Molecular Orbital Methods. XII. Further Extensions of Gaussian-Type Basis Sets for Use in Molecular Orbital Studies of Organic Molecules. *J. Chem. Phys.* **1972**, *56*, 2257−2261.
(60) Hariharan, P. C.; Pople, J. A. Influence of Polarization Functions on Molecular Orbital Hydrogenation Energies. *Theor. Chim. Acta* **1973**, *28*, 213−222.
(61) Clark, T.; Chandrasekhar, J.; Spitznagel, G. W.; Schleyer, P. V. Efficient Diffuse Function-Augmented Basis Sets for Anion Calculations. III. The 3-21+G Basis Set for 1st-Row Elements, Li-F. *J. Comput. Chem.* **1983**, *4*, 294−301.